Secure Task Offloading for Rural Area Surveillance based on UAV-UGV Collaborations

Peipei Chen, Lailong Luo, Deke Guo*, *Senior Member, IEEE,* Xueshan Luo*, Xinyi Li, and Yuchen Sun

Abstract—The increasing availability of autonomous Unmanned Aerial Vehicles (UAVs) has provided an emerging way for extensive surveillance and monitoring in civilian and military with the advantages of high flexibility, mobility, and bird's-eye features. To mitigate the limitations of on-board energy and computation capacity, UAVs usually offload intensive computation tasks (e.g., image/video processing) to base-station-enabled mobile-edge computing (MEC) facilities. However, base stations are not always available in rural areas. To this end, we propose to offload computation-intensive tasks to Unmanned Ground Vehicles (UGVs), which have fixed routes (i.e., highways and roads). However, the UAV-UGV wireless communication may disclose the offloading information to potential eavesdroppers. Besides, such UGVs have sufficient computation slots but may run out of the target area after a period of traveling. In this paper, the tasks cached on UAVs are modeled as a stochastic queue, and a secure communication strategy to offload the cached tasks from UAVs to UGVs is proposed. We try to maximize the average utility of such a UAV-UGV collaboration with respect to latency, power, velocity, anti-collision, and distance. To solve this non-convex mixed integer nonlinear programming problem, a fast converging and computationally efficient iterative algorithm is investigated utilizing the block coordinate descent method and the successive convex approximation technique. Experiments results demonstrate that our algorithm consistently outperforms the state-of-the-art scheme, significantly improving the average utility of the system.

Index Terms—Mobile-edge computing, UAV communication, physical layer security, and area surveillance.

I. INTRODUCTION

Thanks to their mobility, flexibility and bird's-eye features, unmanned aerial vehicles (UAVs) are being increasingly applied in surveillance and data collection [1], [2], in the battlefield, search and rescue, public safety, and border control [3], [4]. Equipped with high-end sensors, high-definition cameras, and GPS, UAVs provide better monitoring perspective than ground networks [5], [6]. However, due to the limited computation capability and on-board power supply, performing computation-intensive tasks (e.g., real-time AI applications, feature extraction, and pattern recognition) on UAVs may not be feasible and even detrimental to their batteries [7], [8]. An existing methodology is to offload the computation-intensive tasks to nearby mobile edge computing (MEC) facilities [9], [10]. Such methodology's mainstream deployment relies on

Peipei Chen, Lailong Luo, Deke Guo, Xueshan Luo, Xinyi Li, and Yuchen Sun are with the Science and Technology on Information Systems Engineering Laboratory, National University of Defense Technology, Changsha, 410073, China. E-mail: {chenpeipei20, luolailong09, dekeguo, xsluo, sunyuchen18}@nudt.edu.cn and lixinyimichael@163.com.

the base stations (BSs) with MEC servers for the offloaded computation [11], where these MEC infrastructures are only available in urban areas. However, more general cases where BSs are missing or nonfunctional (such as disaster/rural areas, borders, battlefields, etc.) are not well studied yet. To explore or monitor such areas with UAVs, more flexible and capable MEC facilities are needed.

Fortunately, unmanned ground vehicles (UGVs), which have advanced communication, storage, and computation modules [7], [12] can meet the demand. UGVs have redundant computation resources and can perform as MEC servers to collaborate with the UAVs nearby their routes. In addition, the UGV might also need UAV surveillance data. For example, in disaster relief tasks, UAVs capture the geomorphic information and send them to UGVs, while UGVs provide disaster rescue based on computing the geomorphic information. Thus, we propose a new MEC-based UAV-UGV collaboration framework, which can be used in disaster rescue, geographic information collection, and moving/static target tracking and detection. In such a framework, the UAVs offload the computation-intensive tasks to available UGVs. As for the UGVs, on the one hand, they are responsible for handling the offload tasks from the UAVs. On the other hand, the UGV may need the UAVs' data for their own duties. However, there are two main challenges in this MEC-based UAV-UGV collaboration framework.

The first challenge is security. The open and frequent air-to-ground communications between UAV and UGV are vulnerable to third-party interception. Specifically, information signals transmitted over UAV communication are more likely to be interrupted by third-party interception. As a result, information leakage becomes an unavoidable concern in outdoor scenarios [13]. For example, the UAVs performing surveillance tasks in rural areas (such as disaster/rural areas, borders, battlefields, etc.) will generate a large number of computation-intensive tasks that need to be offloaded immediately. In practice, although the UAVs can know the eavesdropper's (Eves) estimated location by installing a synthetic aperture radar or camera [7], [14], getting their perfect location is unrealistic. Therefore, the Eves could easily intercept these tasks of UAVs during the offloading process. Although this security problem can be handled by upper-layer encryption in wireless communication, the confidentiality of such an approach relies on the assumptions of computational complexity [15]. Yet such complexity is infeasible for lightweight devices like UAVs that only have limited computation resources [16].

The physical layer security (PLS) [17] is suitable for UAV-UGV communications [18] because of its low complexity. The line-of-sight (LoS) link and the flexibility and mobility

of UAVs bring an opportunity into the PHY design in UAV systems [19]. In particular, a promising approach for UAV systems is a joint design of UAVs' resource allocation and trajectories to enhance PLS [20]. Specifically, on one hand, when a UAV needs to approach eavesdroppers, it can increase its velocity while simultaneously reducing transmission power to degrade the quality of the eavesdropping channel. On the other hand, when the UAV flies close to a UGV, the UAV tries to increase its transmission power and reduce its velocity as possible for improving the transmission rate [21]. To further address the security issues, artificial noise (AN) based PLS is another suitable technology for combating Eves by damaging wiretap channel quality [22], [23]. The UGVs have more power than the UAVs. Therefore, transmitting AN with UGVs is more feasible in our framework.

However, implementing PLS in our UAV-UGV collaboration framework is still a new problem that has not been thoroughly considered. There is a trade-off between the security and computation capability of our MEC-based UAV-UGV collaboration framework. Due to the limited on-board battery of UAVs, scheduling UAV trajectories for enhanced secrecy will undoubtedly increase energy consumption and, in turn, reduce the local computation capacity of UAVs. Additionally, although transmitting AN with UGVs seems promising, there is a risk of vehicles going beyond the communication range, which would expose the signals to the air without protection. Therefore, guaranteeing PLS in our framework remains a challenging problem.

The second challenge is mobility. In our UAV-UGV collaboration framework, both the UAVs in the air and UGVs on the ground are free to move, which enlarges the design space of this framework but also complicates the scheduling of these devices and resources for the surveillance task. The UAVs are allowed to travel freely in the horizontal dimensions, while the UGVs have to follow their own route from the start to the destination. Therefore, we need to ensure that the UAVs and UGVs are within communication range when the tasks are being offloaded.

Due to their mobility, UGVs travel from one place to another, making them available to different UAVs. To meet the requirements of PLS and communication range, UAVs should fly to specific positions so that a portion of their tasks can be offloaded to the UGVs. They should then follow the UGVs for a while to return the calculation results. The positions of UAVs at each time slot need to be determined, taking into account multiple variables such as task scale, latency, computation capacity, UGV speed, and data transmission rate. Moreover, monitoring a place requires frequent video/image processing, which is typically both latency-sensitive and computation-intensive. Therefore, an instant offloading plan needs to be generated for such tasks on the UAVs [8]. The modeling and solving of this problem are extremely complex due to these requirements.

This article introduces a secure cooperation model for the MEC-based UAV-UGV framework. The problem is then formulated as a non-convex mixed-integer nonlinear programming problem (NCMINLP) . Specifically, a utility function is defined to quantify the discrepancy between the generated

secrecy rate of UAV communication and the average area size simultaneously monitored by multiple UAVs. Based on this definition, the trajectory and transmission power of UAVs, as well as the selection and AN power of UGVs, are optimized, considering constraints such as latency, power, velocity, anti-collision, and distance.

To address the intractability of the NCMINLP problem, a lightweight strategy is necessary. In this approach, the original problem is partitioned into six subproblems using the block coordinate descent (BCD) method. Each subproblem is then treated independently, and an alternating optimization technique is employed to solve them. To obtain suboptimal solutions, the successive convex approximation (SCA) technique is utilized in each iteration. Consequently, we present an efficient BCD-based iterative algorithm to find a local optimum with convergence guarantees. In detail, we decompose the original problem into six subproblems, namely, optimization of the UAV trajectory, the UAV transmission power, the AN transmission power, the CPU frequency of the UAV, the CPU frequency of the UGV and the UGV selection. After that, we iterative solve these subproblems with the mentioned strategies. The main contributions are as follows:

1) This is the first work to consider a secure cooperation model for the MEC-based UAV-UGV framework in the presence of multiple Eves. Then, we model this problem as an NCMINLP problem.

2) To solve this NCMINLP problem, we propose a fast converging and computationally efficient iterative algorithm and prove its convergence. Specifically, We decompose the original problem into six subproblems and solve them iteratively with optimization technologies like SCA, BCD, and branch-and-cut.

3) The numerical results consistently demonstrate that the proposed scheme significantly improves the average utility compared to other schemes. To enhance the system's performance, it is possible to efficiently adjust the trajectories, velocities, transmission power, and AN transmission power of the UAVs.

The rest of this paper is organized as follows. Section II reviews the literature relevant to our work. We present the system model and its problem formulation in Section III. In Section IV, an efficient low-complexity algorithm is proposed to obtain the solution. Moreover, simulation results and performance analyses are shown in Section V. Finally, we draw to conclude this paper in Section VI.

II. RELATED WORK

The most relevant work of this paper can be divided into two aspects.

1) Computational Tasks Offloading in Mobile-Edge Computing: A number of works have been studied about computation task offloading problems. To offload the computation-intensive tasks to the MEC server, three aspect problems should be considered: Whether the computation-intensive tasks need to be offloaded at the current time slot? How much transmission power should we use to offload tasks? How to choose a better LoS link to offload tasks? How much computational resources

should we allocate to meet all requirements? There have been some studies on the above issues [24]–[28]. Jiao *et al.* [29] proposes a scheme that jointly optimises the UAV's resource allocation, stochastic computation offloading, and trajectory scheduling to minimise the system's energy consumption. Yuyi *et al.* [24] formulate a problem that joint optimizing computation task offloading scheduling and transmission power to minimize the weighted sum of device energy consumption and tasks processing delay. Tong *et al.* [25] analyses a minimization latency problem by jointly optimizing the tasks computation offloading volume, the multiple user detection matrix and the edge computing resource allocation. Cheng *et al.* [26] and Ning *et al.* [27] propose different throughput optimal schemes for the UAV communication system. Mushu *et al.* [28] propose an optimization approach to utilising the UAVs' energy efficiency in a UAV-assisted MEC system by jointly optimizing the trajectory and resource allocation of UAVs. The above work has studied the performance of the system energy consumption, time delay, resource allocation, and computing rate. But the secure computation offloading issue in terms of rural communications environments has not been worked out well. Fortunately, the secure computation offloading problem falls into the research area of PLS technology.

2) Application of Physical Layer Security (PLS) in UAV Communication: PLS has attracted widespread attention in communication, but its application in UAV communications has just begun [16]. In addition, the mobility of UAVs brings new prospects to PLS technology. Tong *et al.* [8] exploit jamming signals for improving the security of UAV-Edge-Computing Systems. Yi *et al.* [13] design an efficient iterative algorithm to improve the secrecy capacity of the system, which jointly optimizes the UAV location and jamming power, and uses transmission power. Cai *et al.* [30] design a novel UAV-enabled secure communication system by jointly optimizing trajectory and resource design. With the assistance of a cooperative UAV jammer, Wei *et al.* [23] study a secure communication scheme in the system, which solved a worst-case secrecy rate maximization problem. Jiahui *et al.* [31] use a beamforming and collaborative virtual antenna array to achieve secure UAV communications. Cai *et al.* [32] jointly optimise the UAV's trajectory, jamming noise and communication resource allocation to maximize the system energy efficiency. However, current works [23], [30]∼ [32] do not consider the MEC environment. Therefore, how to make full use of PLS techniques in the MEC environment is very necessary. The above works consider computational offloading and secure UAV communication in the MEC-based UAV-UGV collaboration framework. More importantly, no work considers the situation where there is no available BS to act as a server for UAVs. Unlike them, this paper aims to design a feasible scheme to consider secure computation tasks offloading while accomplishing the tasks well in the absence of BSs.

III. Model and Problem Formulation

This section begins by introducing the workflow of the UAV-UGV collaboration for rural area surveillance. It is followed by the modeling and formulation of this problem.
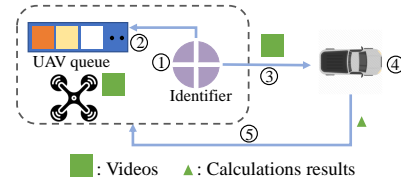

Fig. 1. An example of target detection with UAV-UGV collaboration. The UAV has the task of target detection. ①: Determine whether the task can be offloaded. ②: If offloading is not allowed at this time period, the task will be put into the UAV queue and wait for the next try. ③: Otherwise, the videos will be offloaded to the UGV. ④: The UGV computes the tasks. ⑤: The UGV returns the finding of the target or not.

TABLE I
MAIN TABLE

Notation	Description
$a_{mn}(i)$	the UAV m offload its tasks to UGV n in time slot i
$p_m(i)$	the transmission power of the UAV m at the time slot i
σ^2	the power of additive white gaussian noise
η_0	the channel power gain of LoS link
$\mathbf{q}_m(i)$	the horizontal location of the UAV m
$\widetilde{\mathbf{q}}_k(i)$	the Eve k estimated horizontal location at time slot i
B	the channel bandwidth
ΔQ_k	the maximum estimation error
$R_{mn}(i)$	the rate from the UAV m to the UGV n at time slot i
$R_{mk}(i)$	the rate from the UAV m to the Eve k
$D_m(i)$	the tasks queue backlog of the UAV m at the time slot i
$\Delta D_m(i)$	the size of computation tasks of the UAV m at the time slot i

Each UGV can provide computation services to nearby UAVs while executing their tasks in this system. By contrast, UAVs are responsible for surveillance and data collection while flying around UGVs. Since the UAVs have limited on-board battery and computation resources, the computation-intensive tasks (e.g., image processing or real-time video streaming) can be offloaded to a certain UGV immediately via the wireless transmission link. However, in UAV communication systems, the transmitted confidential information is more likely to be intercepted by multiple independent ground Eves than in terrestrial wireless communication systems. In the whole process of computation offloading, the UGVs need to return the computing results (e.g., timestamp and finding the target or not) to the UAV. However, the offloading time of computed results is small enough to neglect transmission delays, while they are useless for Eves [13], [33]. In addition, if the UGV requires real-time video streaming and image, the computed results do not need to be returned to the UAV. Therefore, this paper mainly focuses on ensuring the secure offloading tasks and efficiently extending the monitoring area. A toy example of UAV-UGV collaboration is given in Fig.1.
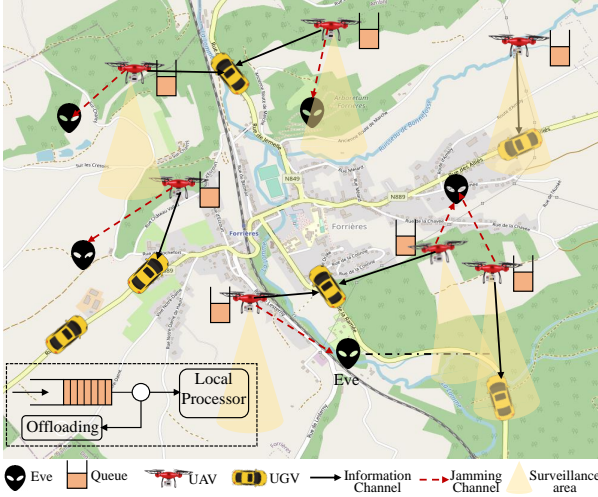
Fig. 2. Illustration of MEC-based UAV-UGV collaboration systems model.

A. System Model

As illustrated in Fig. 2, we consider a MEC-based UAV-UGV collaboration system that includes a set of $\mathcal{M} \triangleq \{1, ..., M\}$ UAVs and $\mathcal{N} \triangleq \{1, ..., N\}$ UGVs in the present of $\mathcal{K} \triangleq \{1, ..., K\}$ Eves. To combat Eves, the full-duplex (FD) UGVs are equipped with double antennas, enabling UGVs to receive confidential UAV signals while transmitting AN. Note that the AN is pre-programmed that just confuses the Eves' listening but does not bring any harm to the UGVs [34]. There are two main communication technologies of UAV communicate with UGV: long-term evolution (LTE) and wifi communication [1]. The wifi range is about hundreds of meters, while LTE is suitable for long-distance fast communication. For ease of reference, the main notations used in this paper are summarized in Table I.

Similar to most existing works [6], [32], a three-dimensional Cartesian coordinate system is used to represent the locations of UAVs, UGVs and Eves. We suppose that UAVs fly at a fixed altitude H [7]. For ease of discussion, the flight period T is evenly divided into I time slots by the length of δ [23]. Accordingly, the location of UAV m at time slot i is denoted by $\mathbf{q}_m(i) = [x_m(i), y_m(i)]^\top \in \mathbb{R}^{2 \times 1}$, with $0 \leq i \leq I$. Additionally, to get the UAV to return to its origin in the end, we assume that each UAV satisfies the constraint $\mathbf{q}_m(0) = \mathbf{q}_m(I), \forall m$.

The horizontal coordinate of the UGV n in time slot i is denoted by: $\bar{\mathbf{q}}_n(i) = [x_n(i), y_n(i)]^\top \in \mathbb{R}^{2 \times 1}$, with $0 \leq i \leq I$. Furthermore, we estimate that the horizontal coordinate of the Eve k is $\widetilde{\mathbf{q}}_k(i) = [x_k(i), y_k(i)]^\top \in \mathbb{R}^{2 \times 1}$, which is imperfectly known by UAVs and UGVs [35]. Similar to literature [13], we consider a bounded error model for Eve locations, expressed as $\widetilde{\mathbf{q}}_k(i) \triangleq \{\|\widetilde{\mathbf{q}}_k(i) - \widehat{\mathbf{q}}_k(i)\| \leq \Delta Q_k\}$, where $\widehat{\mathbf{q}}_k(i)$ indicates the estimated coordinate and ΔQ_k denotes the maximum estimation error. The trajectory constraint of the UAV m need to satisfy:

$$\|\mathbf{q}_m(i+1) - \mathbf{q}_m(i)\|^2 \leq (V_{\max}\delta)^2, i \in \{1, 2, ..., I-1\}, \quad (1)$$

where $V_{\max}$ is the maximum velocity of UAVs. Furthermore, to prevent collision between UAVs, the collision avoidance

constraint [36], i.e,

$$\|\mathbf{q}_m(i) - \mathbf{q}_j(i)\|^2 \geqslant d_{\min}^2, \forall\, i, m, j \neq m, \quad (2)$$

where $d_{\min}$ is the minimum safe distance between two UAVs for anti-collision.

B. Communication Model

For air-to-ground channels, the links from the UAV to the UGV and the Eve are LoS channels [30]. The channel gain from the UAV m to the UGV n and the Eve k at time slot i are $h_{mn}(i)$ and $\bar{h}_{mk}(i)$ respectively, which follows the utilizes a quasi-static block fading channel model [7]. For ground channels, $\widetilde{h}_{nk}(i)$ denotes channel gain at time slot i between the UGV n and the Eve k, which is mainly non-LoS (NLoS) link. It is assumed to constitute both distance-dependent path loss with path-loss exponent $\pi \geq 2$ and small-scale Rayleigh fading [8]. According to the literature [7], [8], the channel gains $h_{mn}(i), \bar{h}_{mk}(i)$ and $\widetilde{h}_{nk}(i)$ can be respectively given as:

$$h_{mn}(i) = \eta_0 d_{mn}^{-2} = \frac{\eta_0}{H^2 + \|\mathbf{q}_m(i) - \bar{\mathbf{q}}_n(i)\|^2}, \quad (3a)$$

$$\bar{h}_{mk}(i) = \eta_0 d_{mk}^{-2} = \frac{\eta_0}{H^2 + \|\mathbf{q}_m(i) - \widetilde{\mathbf{q}}_k(i)\|^2}, \quad (3b)$$

$$\widetilde{h}_{nk}(i) = \eta_0 d_{nk}^{-2} = \frac{\eta_0}{\|\bar{\mathbf{q}}_n(i) - \widetilde{\mathbf{q}}_k(i)\|^\pi}\xi, \quad (3c)$$

where η_0 denotes the unity channel gain at reference distance d ($d = 1$m), and ξ indicates an exponentially distributed random variable with unit mean accounting for the Rayleigh fading.

According to Shannon bound, considering the mutual interference among UAVs, when the UAV m offloads tasks to the UGV n at time slot i, the achievable transmission rate is [37]:

$$R_{mn}(i) = a_{mn}(i) \log_2(1 + \frac{p_m(i)h_{mn}(i)}{\sum\limits_{j \in \mathcal{M}, j \neq m} p_j(i)h_{jn}(i) + \sigma^2}), \quad (4)$$

where $p_m(i)$ denotes the UAV m transmission power, $\sum\limits_{j \in \mathcal{M}, j \neq m} p_j(i)h_{jn}(i)$ means the total interference from all other UAV except UAV m in time slot i and σ^2 is the noise power. If the UAV m offloads its tasks to the UGV n at time slot i, $a_{mn}(i) = 1$; otherwise, $a_{mn}(i) = 0$. Similarly, in time slot i, the instantaneous eavesdropper rate from UAV m to Eve k is computed by:

$$\bar{R}_{mk}(i) = a_{mn}(i) \log_2(1 + \frac{p_m(i)\bar{h}_{mk}(i)}{\psi_{mk}(i)}), \quad (5)$$

where $\psi_{mk}(i) = \sum\limits_{j \in \mathcal{M}, j \neq m} p_j(i)h_{jk}(i) + \sum\limits_{n \in \mathcal{N}} p_n^{an}(i)\widetilde{h}_{nk}(i) + \sigma^2$ and $p_n^{an}(i)$ represents the transmission power of AN from the UGV n at time slot i.

C. Model of Local Computation

In these systems, each UAV can maintain a queueing model for its computation tasks generated by itself, namely tasks queue. The tasks of each UAV can be executed locally or offloaded to a certain UGV. Moreover, the local-computed

tasks are queued in UAV's tasks buffer and will be processed on a first-in-first-out basis [29].

For local computing, if $a_{mn}(i) = 0$, the arriving tasks will be put in queue of UAV m in time slot i. Let $D_m(i)$ be the backlog size of the tasks queue of UAV m at time slot i, $d_m(i)$ denote the computation task executed of the UAV m at time slot i, and $\Delta D_m(i)$ represent the computation tasks of UAV m at time slot i. The tasks generated by UAVs are independent and identically distributed. According to whether the UAV can complete the tasks in the current queue in time slot i, there are two cases:

If $\delta f_m(i) \geq \theta(\Delta D_m(i) + D_m(i))$, we have $d_m(i) = \Delta D_m(i) + D_m(i)$. Thus, the cumulative delay $\lambda_m(i)$ and the computing delay for local computation $T_m^{loc}(i)$ are defined respectively as:

$$\lambda_m(i+1) = 0, \tag{6}$$

$$T_m^{loc}(i+1) = \frac{\theta(\Delta D_m(i)+D_m(i))}{f_m(i)} + \frac{\theta(\lambda_m(i)D_m(i))}{\Delta D_m(i)+D_m(i)}, \tag{7}$$

where $f_m(i)$ represents the CPU frequency of the UAV m at the time slot i and θ denotes the CPU cycles for computing one bit of tasks.

If $\delta f_m(i) < \theta(\Delta D_m(i)+D_m(i))$, we have $d_m(i) = \frac{f_m(i)\delta}{\theta}$. $\lambda_m(i)$ and $T_m^{loc}(i)$ can be redefined respectively as:

$$\lambda_m(i+1) = \frac{\Delta D_m(i)\delta + (D_m(i+1)-\Delta D_m(i))(\delta+\lambda_m(i))}{D_m(i+1)}, \tag{8}$$

$$T_m^{loc}(i+1) = \lambda_m(i) + \delta. \tag{9}$$

As a result, the size of the tasks buffer of UAV m is updated according to the following equation:

$$D_m(i+1) = \max\{D_m(i) - d_m(i), 0\} + \Delta D_m(i), \tag{10}$$

Moreover, the corresponding power consumption for task execution at UAV m is [28]:

$$P_m^{com}(i) = \kappa(f_m(i))^3, \tag{11}$$

in which κ represents the effective switched capacitance.

D. Model of Secure Task Offloading

For tasks offloading, if $a_{mn}(i) = 1$, $\Delta D_{mn}(i)$ bits will be offloaded from UAV m to UGV n at time slot i. In this framework, the UGVs have enough computing power to accomplish the tasks offloaded from UAV in each time slot.

According to Eq.(4), the communication time for task offloading from UAV m to UGV n at time slot i can be calculated as:

$$T_{mn}^{tra}(i) = \frac{\Delta D_{mn}(i)}{BR_{mn}(i)}, \tag{12}$$

where B is the spectrum bandwidth. As a result, after such offloading, the computation time is given by:

$$T_{mn}^{com}(i) = \frac{\Delta D_{mn}(i)\theta}{f_{mn}(i)}, \tag{13}$$

where $f_{mn}(i)$ denotes the idle computing power shared to the UAV m by UGV n at the time slot i. Based on Eqs. (12) and (13), the total time of completing these tasks with a UAV-UGV collaboration:

$$T_{mn}^{off}(i) = T_{mn}^{tra}(i) + T_{mn}^{com}(i). \tag{14}$$

Similar to the literature [33], the transmission time of computed results is small enough to be ignored. In addition, the power consumption of the UGV n for task execution at time slot i can be described as:

$$P_{mn}^{com}(i) = \varepsilon(f_{mn}(i))^3, \tag{15}$$

where ε is the effective switched capacitance of the UGV. Consequently, $P_n^{com}(i) = \sum_{i=1}^{M} P_{mn}^{com}(i)$.

E. The Coverage Utility Function of UAVs

The overlapping monitoring areas of multiple UAVs need to be optimized for monitoring an area better. To understand the area of monitoring overlapping more clearly, the illustration of overlapping areas is shown in Fig. 3. We assume the monitoring radius of a UAV is R, and the monitoring area is πR^2. The distance between the UAV m and UAV j at time slot i is $d_{mj}(i)$. There has no overlapping area when $d_{mj} \geq 2R$; otherwise, the overlapping area of monitoring is the overlapping area between two circles. As a result, we define the overlapping area of monitoring between the UAV m and j as:

$$\begin{cases} \zeta_{mj}(i) = \varphi(i) & d_{mj}(i) < 2R \\ \zeta_{mj}(i) = 0 & d_{mj}(i) \geqslant 2R \end{cases} \tag{16}$$

where the $\varphi(i)$ represents the overlapping area of monitoring, which can be presented as $\varphi(i) = 2R^2 \arccos \frac{d_{mj}(i)}{2R} - d_{mj}(i)\sqrt{R^2 - \frac{(d_{mj}(i))^2}{4}}$, and $d_{mj}(i) = \|\mathbf{q}_m(i) - \mathbf{q}_j(i)\|$. Consequently, the average overlapping area over I time slots can be following denoted as $\zeta = \frac{1}{I} \sum_{i=1}^{I} \zeta_{mj}(i)$.
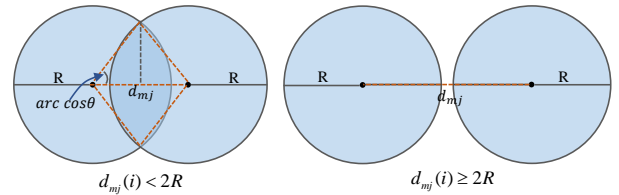

Fig. 3. An example of the overlapping area of two UAVs.

F. Problem Formulation

To improve the security of confidential information transmission while performing the surveillance tasks efficiently, we define an average utility function as $\vartheta = \frac{1}{I} \sum_{i=1}^{I} \sum_{m=1}^{M} \left[R_{mn}(i) - \max_{k \in \mathcal{K}} \bar{R}_{mk}(i) \right]^+ - \tau\zeta$, in which the $\frac{1}{I} \sum_{i=1}^{I} \sum_{m=1}^{M} \left[R_{mn}(i) - \max_{k \in \mathcal{K}} \bar{R}_{mk}(i) \right]^+$ represents the average secrecy rate, ζ denotes average overlapping areas for monitoring, and τ is the weight coefficient. The goal of this paper is to maximize the minimum average utility over T period by jointly optimizing the UAVs trajectory $\mathbf{Q} =$

$\{\mathbf{q}_m(i), V_m(i), \forall m, i\}$, the transmission power of the UAV $\mathbf{P}_m = \{p_m(i), \forall m, i\}$, the AN transmission power of the UGV n $\bar{\mathbf{P}}_n = \{p_n^{an}(i), \forall n, i\}$, the CPU frequency of the UAV $\mathbf{F}_m = \{f_m(i), \forall m, n, i\}$, the CPU frequency of the UGV $\bar{\mathbf{F}}_n = \{\bar{f}_n(i), \forall m, n, i\}$, and the UGVs selection $\mathcal{A} = \{a_{mn}(i), \forall m, n, i\}$, subject to the tasks latency, UAV mobility, anti-collision and power constraints. Thus, the optimization problem can be formulated as:

$$\max_{\mathbf{Q}, \mathbf{P}_m, \bar{\mathbf{P}}_n, \mathbf{F}_m, \bar{\mathbf{F}}_n, \mathcal{A}} \vartheta \tag{17a}$$

$$\text{s.t.} \frac{1}{I}\sum_{i=1}^{I}\sum_{m=1}^{M}\left[R_{mn}(i) - \max_{k\in\mathcal{K}}\bar{R}_{mk}(i)\right]^+ - \tau\zeta \geq \vartheta, \forall n, \tag{17b}$$

$$\frac{1}{I}\sum_{i=1}^{I}T_m^{loc}(i) \leq T, \forall m, \tag{17c}$$

$$\frac{1}{I}\sum_{i=1}^{I}T_{mn}^{off}(i) \leq T, \forall m, n, \tag{17d}$$

$$p_m(i) + P_m^{com}(i) \leq P_m^{\max}, \forall m, i, \tag{17e}$$

$$p_n^{an}(i) + P_n^{com}(i) \leq P_n^{\max}, \forall n, i, \tag{17f}$$

$$\sum_{n=1}^{N} a_{mn}(i) \leq 1, \forall m, i, \tag{17g}$$

$$\mathbf{q}_m(0) = \mathbf{q}_m(I), \forall m, \tag{17h}$$

$$\|\mathbf{q}_m(i+1) - \mathbf{q}_m(i)\|^2 \leq (V_{\max}\delta)^2, \forall m, i = 1, ..., I-1, \tag{17i}$$

$$\|\mathbf{q}_m(i) - \mathbf{q}_j(i)\|^2 \geqslant d_{\min}^2, \forall m, i, j \neq m, \tag{17j}$$

$$\|\mathbf{q}_m(i+1) - \mathbf{q}_m(i)\|^2 \geqslant d_m^2, \forall m, i, \tag{17k}$$

where the constraints (17c) and (17d) denote the delay constraints for the tasks; the constraints (17e) and (17f) represent the maximum power constraint of the UAV and UGV, respectively; the constraint (17g) ensures the UAV m is served by most one UGV at each time slot; the constraints (17h) and (17i) are the UAV mobility constraints; the constraint (17j) ensures that all UAVs can avoid the collision; and constraint (17k) is to increase UAVs' coverage and avoid UAVs moving too close in each time slot.

Firstly, the discrete variable $\mathcal{A}$ for selecting UGV is binary. Secondly, $R_{mn}(i)$ and $\max_{k\in\mathcal{K}}\bar{R}_{mk}(i)$ in the objective function are highly nonlinear due to their dependent UAV trajectory variable $\mathbf{Q}$. Thirdly, the imperfect location of the Eves $(\Delta x_k(i), \Delta y_k(i))$ imposes semi-infinite number of constraints, which makes it more complicated. Therefore, the problem (17) is an NCMINLP problem that is challenging to solve optimally.

IV. THE PROPOSED ITERATIVE ALGORITHM

Since the indeterminate locations of Eves result in an semi-infinite number of constraints for this complex problem, it is necessary to simplify the constraints associated with Eves' locations. Considering the estimation error ΔQ_k of the Eve k, we define $\bar{R}_{mk}^{up}(i)$ as the upper bound for the achieved rate of the Eve k from the UAV m. This upper bound can be given by:

$$\bar{R}_{mk}^{up}(i) = \log_2\left(1 + \frac{p_m(i)\bar{h}_{mk}^*(i)}{\psi_{mk}(i) + \sum_{n\in\mathcal{N}} p_n^{an}(i)\widetilde{h}_{nk}^*(i)}\right), \tag{18}$$

where $\psi_{mk}(i) = \sum_{j\in\mathcal{M}, j\neq m} p_j(i)h_{jk}^*(i) + \sigma^2$, $\bar{h}_{mk}^*(i)$ and $\widetilde{h}_{nk}^*(i)$ are chosen to maximize $\bar{R}_{mk}^{up}(i)$. According to the formula $\widetilde{\mathbf{q}}_k(i) \triangleq \{\|\widetilde{\mathbf{q}}_k(i) - \widehat{\mathbf{q}}_k(i)\| \leq \Delta Q_k\}$, the closed-form solutions of $\bar{h}_{mk}^*(i)$ and $\widetilde{h}_{nk}^*(i)$ can be derived as follows:

$$\bar{h}_{mk}^*(i) = \max_{k\in\mathcal{K}} \frac{\eta_0}{H^2 + (\sqrt{(x_m(i) - x_k(i))^2 + (y_m(i) - y_k(i))^2} - \Delta Q_k)^2}, \tag{19a}$$

$$\widetilde{h}_{nk}^*(i) = \min_{k\in\mathcal{K}} \frac{\eta_0}{(\sqrt{(x_n(i) - x_k(i))^2 + (y_n(i) - y_k(i))^2} + \Delta Q_k)^2}. \tag{19b}$$

According to studies [13] and [38], the joint optimization always brings about a non-negative secrecy capacity, so the $[\cdot]^+$ operator on the objective function can be omitted without affecting the solution. Thus, the problem (17) can be simplified as:

$$\max_{\mathbf{Q}, \mathbf{P}_m, \bar{\mathbf{P}}_n, \mathbf{F}_m, \bar{\mathbf{F}}_n, \mathcal{A}} \vartheta$$

$$\text{s.t.} \frac{1}{I}\sum_{i=1}^{I}\sum_{m=1}^{M}(R_{mn}(i) - R_0) - \tau\zeta \geq \vartheta, \forall n, \tag{20}$$

$$\bar{R}_{mk}^{up}(i) \leqslant R_0, \forall m, k, i,$$

$$(17c) - (17k),$$

where R_0 is the auxiliary variables [39]. Then, we partition the problem (20) into six subproblems by the BCD technique, i.e., alternately optimizing different groups of the UAV trajectory $\mathbf{Q}$, the UAV transmission power $\mathbf{P}_m$, the AN transmission power of the UGV $\bar{\mathbf{P}}_n$, the CPU frequency of the UAV $\mathbf{F}_m$, the CPU frequency of the UGV $\bar{\mathbf{F}}_n$, and UGV selection $\mathcal{A}$ while fixing the other variables.

A. Optimization of the UAV Trajectory $\mathbf{Q}$

For fixed $\mathbf{P}_m$, $\bar{\mathbf{P}}_n$, $\mathbf{F}_m$, $\bar{\mathbf{F}}_n$, and $\mathcal{A}$, the subproblem for optimizing the UAV trajectory $\mathbf{Q}$ can be formulated as:

$$\max_{\vartheta, \mathbf{Q}} \vartheta \tag{21a}$$

$$\text{s.t.} \frac{1}{I}\sum_{i=1}^{I}\sum_{m=1}^{M}(R_{mn}(i) - R_0) - \tau\zeta \geq \vartheta, \forall n, \tag{21b}$$

$$\bar{R}_{mk}^{up}(i) \leqslant R_0, \forall m, k, i, \tag{21c}$$

$$\frac{1}{I}\sum_{i=1}^{I}T_m^{loc}(i) \leq T, \forall m, \tag{21d}$$

$$\frac{1}{I}\sum_{i=1}^{I}T_{mn}^{off}(i) \leq T, \forall m, n, \tag{21e}$$

$$\mathbf{q}_m(0) = \mathbf{q}_m(I), \forall m, \tag{21f}$$

$$\|\mathbf{q}_m(i+1) - \mathbf{q}_m(i)\|^2 \leq (V_{\max}\delta)^2, \forall m, i = 1, ..., I-1, \tag{21g}$$

$$\|\mathbf{q}_m(i) - \mathbf{q}_j(i)\|^2 \geqslant d_{\min}^2, \forall m, i, j \neq m, \tag{21h}$$

$$\|\mathbf{q}_m(i+1) - \mathbf{q}_m(i)\|^2 \geqslant d_m^2, \forall m, i, j \neq m. \tag{21i}$$

Since the nonconvexity of the constraints (21b), (21c), (21h) and (21i), the subproblem (21) is nonconvex, which is difficult

to be solved directly. Fortunately, the subproblem (21) can be transformed into convex by SCA technique, the transformed process see Appendix A. Based on this, the problem (21) can be reformulated as:

$$\max_{\vartheta, \mathbf{Q}, \mathbf{S}} \vartheta \tag{22a}$$

$$\text{s.t.} \quad \frac{1}{I} \sum_{i=1}^{I} \sum_{m=1}^{M} (\bar{R}_{mn}(i) - R_0) - \tau\zeta \geq \vartheta, \forall n, \tag{22b}$$

$$\bar{R}_{mk}^{up}(i) \leqslant R_0, \forall m, k, i, \tag{22c}$$

$$\frac{1}{I} \sum_{i=1}^{I} T_m^{loc}(i) \leq T, \forall m, \tag{22d}$$

$$\frac{1}{I} \sum_{i=1}^{I} \left(T_{mn}^{off}(i)\right) \leq T, \forall m, n, \tag{22e}$$

$$d_{\min}^2 \leqslant S_f, \tag{22f}$$

$$d_m^2 \leqslant S_g, \tag{22g}$$

$$\mathbf{q}_m(0) = \mathbf{q}_m(I), \forall m, \tag{22h}$$

$$\|\mathbf{q}_m(i+1) - \mathbf{q}_m(i)\|^2 \leq (V_{\max}\delta)^2, \forall m, i = 1, ..., I-1, \tag{22i}$$

where $\mathbf{S} = \{S_{mk}(i), \forall m, k, i\}$,

$$S_f = -\left\|\mathbf{q}_m^r(i) - \mathbf{q}_j^r(i)\right\|^2 + 2(\mathbf{q}_m^r(i) - \mathbf{q}_j^r(i))$$
$$\mathbf{q}_m(i) - \mathbf{q}_j(i)), \forall m, i, j \neq m$$
$$S_g = -\|\mathbf{q}_m^r(i+1) - \mathbf{q}_m^r(i)\|^2 + 2(\mathbf{q}_m^r(i+1)$$
$$- \mathbf{q}_m^r(i))(\mathbf{q}_m(i+1) - \mathbf{q}_m(i)), \forall m, i = 1, ..., I-1,$$
$$S_h = (\|\mathbf{q}_m^r(i) - \widetilde{\mathbf{q}}_k(i)\| - \Delta Q)^2 + 2(\|\mathbf{q}_m^r(i) - \widetilde{\mathbf{q}}_k(i)\|$$
$$- \Delta Q)\frac{(\mathbf{q}_m^r(i) - \widetilde{\mathbf{q}}_k(i))^\top}{\|\mathbf{q}_m^r(i) - \widetilde{\mathbf{q}}_k(i)\|}(\mathbf{q}_m(i) - \mathbf{q}_m^r(i)), \forall m, k, i.$$

After the above reformulation, it can be observed that the left-hand-side of constraint (22b) is jointly concave with respect to $\mathbf{q}_m(i)$, which is a convex variable. Furthermore, the constraints (22c), (22f), and (22g) are convex, while the remaining constraints are linear in nature. As a result, the problem (22) can be efficiently solved using standard convex optimization solvers, e.g., CVX [40].

B. Optimization of the UAV Transmission Power $\boldsymbol{P}_m$

For fixed $\mathbf{Q}$, $\bar{\mathbf{P}}_n$, $\mathbf{F}_m$, $\bar{\mathbf{F}}_n$, and $\mathcal{A}$, the subproblem for optimizing the transmission power of UAV $\mathbf{P}_m$ can be formulated as:

$$\max_{\vartheta, \mathbf{P}_m} \vartheta \tag{23a}$$

$$\text{s.t.} \quad \frac{1}{I} \sum_{i=1}^{I} \sum_{m=1}^{M} (R_{mn}(i) - R_0) - \tau\zeta \geq \vartheta, \forall n, \tag{23b}$$

$$\bar{R}_{mk}^{up}(i) \leqslant R_0, \forall m, k, i \tag{23c}$$

$$\frac{1}{I} \sum_{i=1}^{I} T_{mn}^{off}(i) \leq T, \forall m, n, \tag{23d}$$

$$p_m(i) + P_m^{com}(i) \leq P_m^{\max}, \forall m, i. \tag{23e}$$

Due to the nonconvexity of constraints (23b) and (23c), the problem (23) is nonconvex. However, it can be transformed into a convex problem by applying the SCA technique. The detailed transformation process is provided in Appendix B. After applying the SCA technique, the problem (23) can be re-expressed as the following problem:

$$\max_{\vartheta, \mathbf{P}_m} \vartheta \tag{24a}$$

$$\text{s.t.} \quad \frac{1}{I} \sum_{i=1}^{I} \sum_{m=1}^{M} (I_1(i) - I_2(i) - R_0) - \tau\zeta \geq \vartheta, \forall n, \tag{24b}$$

$$I_3(i) - I_4(i) \leq R_0, \forall m, k, i, \tag{24c}$$

$$\frac{1}{I} \sum_{i=1}^{I} \left(T_{mn}^{off}(i)\right) \leq T, \forall m, n, \tag{24d}$$

$$p_m(i) \leq P_m^{\max}, \forall m, i, \tag{24e}$$

where I_1, I_2, I_3 and I_4 see Appendix B. Now, the Eq. (24) is a convex optimization problem that existing general convex optimizer can efficiently solve.

C. Optimization of the AN Transmission power $\bar{\boldsymbol{P}}_n$

By fixed $\mathbf{Q}$, $\mathbf{P}_m$, $\mathbf{F}_m$, $\bar{\mathbf{F}}_n$ and $\mathcal{A}$, the third subproblem for optimizing the AN transmission power $\bar{\mathbf{P}}_n$ can be written as:

$$\max_{\vartheta, \bar{\mathbf{P}}_n} \vartheta \tag{25a}$$

$$\text{s.t.} \quad \frac{1}{I} \sum_{i=1}^{I} \sum_{m=1}^{M} (R_{mn}(i) - R_0) - \tau\zeta \geq \vartheta, \forall n, \tag{25b}$$

$$\bar{R}_{mk}^{up}(i) \leqslant R_0, \forall m, k, i, \tag{25c}$$

$$p_n^{an}(i) + P_n^{com}(i) \leq P_n^{\max}, \forall n, i, \tag{25d}$$

It is obvious that Eq. (25) is a convex optimization problem that can be efficiently solved by a general convex optimizer.

D. Optimization of the CPU frequency of the UAV $\boldsymbol{F}_m$

For any given $\mathbf{Q}$, $\mathbf{P}_m$, $\bar{\mathbf{P}}_n$, $\bar{\mathbf{F}}_n$ and $\mathcal{A}$, the fourth subproblem for optimizing the CPU frequency of UAV can be expressed as:

$$\min_{\mathbf{F}_m} \mathbf{F}_m \tag{26a}$$

$$\text{s.t. } (17c), (17e) \tag{26b}$$

Note that the problem (26) is a linear optimization problem, which can be efficiently solved.

E. Optimization of the CPU frequency of the UGV $\bar{\boldsymbol{F}}_n$

For any given $\mathbf{Q}$, $\mathbf{P}_m$, $\bar{\mathbf{P}}_n$, $\mathbf{F}_m$ and $\mathcal{A}$, the fifth subproblem for optimizing the CPU frequency of UGV is formulated as:

$$\min_{\bar{\mathbf{F}}_n} \bar{\mathbf{F}}_n \tag{27a}$$

$$\text{s.t. } (17d), (17f) \tag{27b}$$

Similarly, the problem (27) can be efficiently solved, because it is a linear optimization problem.

F. Optimization of the UGV Selection $\mathcal{A}$

For given $\mathbf{Q}$, $\mathbf{P}_m$, $\bar{\mathbf{P}}_n$, $\mathbf{F}_m$, and $\bar{\mathbf{F}}_n$, the subproblem of UGV selection is formulated as:

$$\max_{\vartheta, \mathcal{A}} \ \vartheta \tag{28a}$$

$$\text{s.t. } a_{mn}(i)\varrho_{mn} + (1 - a_{mn}(i))L \geq \vartheta, \forall m, n, i, \tag{28b}$$

$$p_n^{an}(i) + P_n^{com}(i) \leq P_n^{\max}, \forall n, i, \tag{28c}$$

$$\sum_{n=1}^{N} a_{mn}(i) \leq 1, \forall m, i, \tag{28d}$$

$$\frac{1}{I} \sum_{i=1}^{I} T_{mn}^{off}(i) \leq T, \forall m, n, \tag{28e}$$

where $\varrho_{mn} = \frac{1}{I} \sum_{i=1}^{I} \sum_{m=1}^{M} (R_{mn}(i) - R_0) - \tau\zeta$, and L is bigger than the upper bound of ϑ. Since the decision variable $a_{mn}(i)$ is binary, the subproblem of UGV selection can be solved efficiently by the branch-and-cut method. Next, we need to determine whether the selected UGV meets the requirements.

Due to the mobility of UAVs and UGVs, UAVs may not communicate with all UGVs during data transmission. Therefore, if the computation tasks of the UAV m can be offloaded to the UGV n in time slot i, the following inequality must be meet $\frac{\Delta D_m(i)}{R_{mn}(i)} \leqslant \delta$. To address the optimization of the task offloading, Algorithm 1 is proposed. Specifically, let $\mathcal{D} = \Delta D_m(i)$ denote the size of arrived computation tasks of each UAV at time slot i. Note that a sufficient transmission rate should be reserved for offloading computation tasks (lines 3-12). Consequently, in advance, we need to judge whether the tasks generated by UAVs can be uploaded to the UGV successfully (lines 7 and 9).

Algorithm 1 Task offloading Optimization Algorithm

1: Input: $\mathcal{D}, R_{mn}(i), B$
2: $\mathcal{A} = \mathbf{0}, i = 0, m = 1$;
3: **for** $m \leqslant \mathcal{M}$ **do**
4:     **for** $i \leqslant I$ **do**
5:         Select UGV n based on Equ.(28)
6:         Calculate $R_{mn}(i)$ based on Equ.(4)
7:         **if** $\mathcal{D}(i, m) \leqslant BR_{mn}(i)\delta$ **then**
8:             $\mathcal{A}(i, m) = 1$;
9:         **else**
10:            $\mathcal{A}(i, m) = 0$;
11:         **end if**
12:     **end for**
13: **end for**
14: Return: $\mathcal{A}$

G. Overall Algorithm 2 and Convergence

From the above discussion, we propose a BCD-based iterative optimization algorithm for the problem (20) in Algorithm 2 by utilizing the BCD method, SCA technique, and branch-and-cut method. In detail, the optimization variables in the original problem (20) are divided into six blocks. Then, $\mathbf{Q}$, $\mathbf{P}_m$, $\bar{\mathbf{P}}_n$, $\mathbf{F}_m$, $\bar{\mathbf{F}}_n$, and $\mathcal{A}$ are alternately optimized by solving problems (22), (24), (25), (26), (27) and (28) respectively. For

---

Algorithm 2 BCD-based Iterative Optimization Algorithm for problem (20)

1: Initialize $r = 0$, $\mathbf{Q}^r, \mathbf{P}_m^r, \bar{\mathbf{P}}_n^r, \mathbf{F}_m^r, \bar{\mathbf{F}}_n^r, \mathcal{A}^r$, and the convergence accuracy κ.
2: **repeat**
3:     Solve problem (22) with $\{\mathbf{P}_m^r, \bar{\mathbf{P}}_n^r, \mathbf{F}_m^r, \bar{\mathbf{F}}_n^r, \mathcal{A}^r\}$, and obtain $\mathbf{Q}^{r+1}$;
4:     Solve problem (24) with $\{\mathbf{Q}^{r+1}, \bar{\mathbf{P}}_n^r, \mathbf{F}_m^r, \bar{\mathbf{F}}_n^r, \mathcal{A}^r\}$, and obtain $\mathbf{P}_m^{r+1}$;
5:     Solve problem (25) with $\{\mathbf{Q}^{r+1}, \mathbf{P}_m^{r+1}, \mathbf{F}_m^r, \bar{\mathbf{F}}_n^r, \mathcal{A}^r\}$, and obtain $\bar{\mathbf{P}}_n^{r+1}$;
6:     Solve problem (26) with $\{\mathbf{Q}^{r+1}, \mathbf{P}_m^{r+1}, \bar{\mathbf{P}}_n^{r+1}, \bar{\mathbf{F}}_n^r, \mathcal{A}^r\}$, and obtain $\mathbf{F}_m^{r+1}$;
7:     Solve problem (27) with $\{\mathbf{Q}^{r+1}, \mathbf{P}_m^{r+1}, \bar{\mathbf{P}}_n^{r+1}, \mathbf{F}_m^{r+1}, \mathcal{A}^r\}$, and obtain $\bar{\mathbf{F}}_n^{r+1}$;
8:     Solve problem (28) with $\{\mathbf{Q}^{r+1}, \mathbf{P}_m^{r+1}, \bar{\mathbf{P}}_n^{r+1}, \mathbf{F}_m^{r+1}, \bar{\mathbf{F}}_n^{r+1}\}$, and obtain $\mathcal{A}^{r+1}$;
9:     Update $r = r + 1$;
10: **until** The objective value increase is lower than convergence accuracy κ.

---

the first three subproblems, we iterative compute the local optimum of the convex problem by updating the initial feasible solutions until a stationary solution of the original nonconvex problem is found. In addition, the solution generated in each iteration is input to the next iteration for each subproblem. The detailed process is summarized in Algorithm2. Since we only solve approximate problems (22), (24), (25), (26), (27) and (28) optimally, the convergence of Algorithm 2 need to be demonstrated.

Proposition 1: Algorithm 2 is convergent.

Proof: Supposing $\vartheta\{\mathbf{Q}^r, \mathbf{P}_m^r, \bar{\mathbf{P}}_n^r, \mathbf{F}_m^r, \bar{\mathbf{F}}_n^r, \mathcal{A}^r\}$ is the objective value of the problem (20) in the rth iteration. First, for given $\mathbf{P}_m^r, \bar{\mathbf{P}}_n^r, \mathbf{F}_m^r, \bar{\mathbf{F}}_n^r$, and $\mathcal{A}^r$ in step 3 of Algorithm 2, the optimal solution of (22) is obtained. We have:

$$\vartheta\{\mathbf{Q}^r, \mathbf{P}_m^r, \bar{\mathbf{P}}_n^r, \mathbf{F}_m^r, \bar{\mathbf{F}}_n^r, \mathcal{A}^r\} \overset{(a)}{=} \vartheta_{trj}^{lb,r}\{\mathbf{Q}^r, \mathbf{P}_m^r, \bar{\mathbf{P}}_n^r, \mathbf{F}_m^r, \bar{\mathbf{F}}_n^r, \mathcal{A}^r\}$$

$$\overset{(b)}{\leq} \vartheta_{trj}^{lb,r}\{\mathbf{Q}^{r+1}, \mathbf{P}_m^r, \bar{\mathbf{P}}_n^r, \mathbf{F}_m^r, \bar{\mathbf{F}}_n^r, \mathcal{A}^r\}$$

$$\overset{(c)}{\leq} \vartheta\{\mathbf{Q}^{r+1}, \mathbf{P}_m^r, \bar{\mathbf{P}}_n^r, \mathbf{F}_m^r, \bar{\mathbf{F}}_n^r, \mathcal{A}^r\} \tag{29}$$

where $\vartheta_{trj}^{lb,r}$ denotes the objective value of the problem (22), (a) holds since the tightness of the first-order Taylor expansions at local points in the problem (21), (b) holds since in step 3 the problem (22) is solved for given $\mathbf{P}_m^r, \bar{\mathbf{P}}_n^r, \mathcal{A}^r$, and (c) holds since the objective value of the problem (22) is the lower bound of the problem (21). Second, for given $\mathbf{Q}^{r+1}, \bar{\mathbf{P}}_n^r, \mathbf{F}_m^r, \bar{\mathbf{F}}_n^r$ and $\mathcal{A}^r$ in step 4, we have:

$$\begin{aligned} &\vartheta\{\mathbf{Q}^{r+1}, \mathbf{P}_m^r, \bar{\mathbf{P}}_n^r, \mathbf{F}_m^r, \bar{\mathbf{F}}_n^r, \mathcal{A}^r\} \\ &= \vartheta_p^{lb,r}\{\mathbf{Q}^{r+1}, \mathbf{P}_m^r, \bar{\mathbf{P}}_n^r, \mathbf{F}_m^r, \bar{\mathbf{F}}_n^r, \mathcal{A}^r\} \\ &\leq \vartheta_p^{lb,r}\{\mathbf{Q}^{r+1}, \mathbf{P}_m^{r+1}, \bar{\mathbf{P}}_n^r, \mathbf{F}_m^r, \bar{\mathbf{F}}_n^r, \mathcal{A}^r\} \\ &\leq \vartheta\{\mathbf{Q}^{r+1}, \mathbf{P}_m^{r+1}, \bar{\mathbf{P}}_n^r, \mathbf{F}_m^r, \bar{\mathbf{F}}_n^r, \mathcal{A}^r\}, \end{aligned} \tag{30}$$

where $\vartheta_p^{lb,r}$ denotes the objective value of problem (24). Similar to the problem (29), the solution to problem (30) at

$r + 1$th is also less than the solution at rth. Thus, the original subproblem (23) is non-decreasing. Third, for given $\mathbf{Q}^{r+1}$, $\mathbf{P}_m^{r+1}, \mathbf{F}_m^r, \bar{\mathbf{F}}_n^r$ and $\mathcal{A}^r$ in step 5 of the Algorithm 2, we have:

$$\vartheta\{\mathbf{Q}^{r+1}, \mathbf{P}_m^{r+1}, \bar{\mathbf{P}}_n^r, \mathbf{F}_m^r, \bar{\mathbf{F}}_n^r, \mathcal{A}^r\} \leqslant \vartheta\{\mathbf{Q}^{r+1}, \mathbf{P}_m^{r+1}, \bar{\mathbf{P}}_n^{r+1}, \mathbf{F}_m^r, \bar{\mathbf{F}}_n^r, \mathcal{A}^r\}. \tag{31}$$

Similarly, in steps 6, step 7, and step 8 of Algorithm 2, since the subproblems (26) and (27) are not in the objective function, the objective value is unchanged after each iteration. Therefore, we obtain:

$$\vartheta\{\mathbf{Q}^{r+1}, \mathbf{P}_m^{r+1}, \bar{\mathbf{P}}_n^{r+1}, \mathbf{F}_m^r, \bar{\mathbf{F}}_n^r, \mathcal{A}^r\} = \vartheta\{\mathbf{Q}^{r+1}, \mathbf{P}_m^{r+1}, \bar{\mathbf{P}}_n^{r+1}, \mathbf{F}_m^{r+1}, \bar{\mathbf{F}}_n^{r+1}, \mathcal{A}^r\}. \tag{32}$$

Finally, since the $\mathcal{A}$ is global optimization solution for subproblem (28) with given $\mathbf{Q}^{r+1}, \mathbf{P}_m^{r+1}, \bar{\mathbf{P}}_n^{r+1}, \mathbf{F}_m^{r+1}, \bar{\mathbf{F}}_n^{r+1}$ in step 8 of Algorithm 2, we have:

$$\vartheta\{\mathbf{Q}^{r+1}, \mathbf{P}_m^{r+1}, \bar{\mathbf{P}}_n^{r+1}, \mathbf{F}_m^r, \bar{\mathbf{F}}_n^r, \mathcal{A}^r\} \leqslant \vartheta\{\mathbf{Q}^{r+1}, \mathbf{P}_m^{r+1}, \bar{\mathbf{P}}_n^{r+1}, \mathbf{F}_m^{r+1}, \bar{\mathbf{F}}_n^{r+1}, \mathcal{A}^{r+1}\}. \tag{33}$$

According to (29)-(33), we can conclude:

$$\vartheta\{\mathbf{Q}^r, \mathbf{P}_m^r, \bar{\mathbf{P}}_n^r, \mathbf{F}_m^r, \bar{\mathbf{F}}_n^r, \mathcal{A}^r\} \leqslant \vartheta\{\mathbf{Q}^{r+1}, \mathbf{P}_m^{r+1}, \bar{\mathbf{P}}_n^{r+1}, \mathbf{F}_m^{r+1}, \bar{\mathbf{F}}_n^{r+1}, \mathcal{A}^{r+1}\}. \tag{34}$$

which can guarantee that the objective value of problem (20) is non-decreasing after each iteration. In algorithm 2, we use $\|\vartheta^{r+1} - \vartheta^r\}\|$ to measure the stationary. Thus, the iteration termination when $\|\vartheta^{r+1} - \vartheta^r\}\| \leqslant \kappa$, where κ is the desired accuracy. When the objective value increment of problem (20) is lower than convergence accuracy κ, the upper bound of the objective value of problem (20) is a finite value. Thus, the proposed Algorithm 2 is guaranteed to converge.

H. Complexity analysis of Algorithm 2

The computational complexity of proposed BCD-based Algorithm 2 focuses on optimizing $\mathbf{Q}, \mathbf{P}_m, \mathbf{P}_n, \mathbf{F}_m, \bar{\mathbf{F}}_n, \mathcal{A}$ in problems (22), (24), (25), (26), (27) and (28), respectively. The complexity of algorithm 2 mainly depends on the number of variables. The sub-problems can be solved by the interior point method in steps 3 and 4. As is known to all, the complexity of the interior point method is $\mathcal{O}(E^{3.5} \log \frac{1}{\omega})$, where the ω is defined as convergence accuracy and E means variable dimension. Algorithm 2 has the variables of N UGVs, K Eves, and I time slots. Thus, $3NKI$ variables need to optimize. As a result, the complexity of steps 3 and 4 is $\mathcal{O}((3NKI)^{3.5} \log \frac{1}{\omega} Z)$, where Z means the iteration number. In steps 5, 6, and 7, the subproblems are directly solved. Therefore, the complexity of solving problems (25), and (26) can be ignored. In step 8, the complexity of the problem (28) is $2MN$. In conclusion, the computational complexity of Algorithm 2 is $\mathcal{O}((3NKI)^{3.5} \log \frac{1}{\omega} Z) + 2MN$.

V. NUMERICAL RESULTS

In this section, we first introduce the evaluation methodology and then detail the performance of the involved schemes.

A. Experiment Settings

1) Experiment Configuration: We consider the systems with $\mathcal{N} = 10$ UGVs distributed in an area of 1000×1000 m². The trajectories of UGV are randomly selected from the dataset of TAPASCologne project [1]. Due to the importance of the initial scheme for Algorithm 2, we let the initial trajectory of each UAV as a circular, based on the suggestion from literature [36]. Each UAV executes the assigned tasks with the volume of $\mathcal{D}(i, m)$ at each time slot. The $\mathcal{D}(i, m)$ follows a uniform distribution within $[0, \mathcal{D}_{\max}]$. Unless otherwise specified, there are three Eves, and their estimated locations are set to $\text{Eve}_1 = [250, 250]^\top$, $\text{Eve}_2 = [650, 850]^\top$, and $\text{Eve}_3 = [800, 600]^\top$, respectively. The flight duration of the UAVs $T = 75$ s. As a footnote, the $\mathbf{P}_m^0$ represents initial transmission power of the UAV m and $\bar{\mathbf{P}}_n^0$ means initial AN transmission power of the UGV n. Other parameters are summarized in Table II [13], [29], [36].

TABLE II
SIMULATION VALUE SETTING.

Notations	Value	Notations	value
$\mathcal{D}_{\max}$	0.15 Mb	$d_{\min}$	50 m
I	100	$\bar{\mathbf{P}}_n^0$	0.9 W
d_{m}	10 m	$V_{\max}$	30 m/s
η_0	-30 dB	$\bar{\mathbf{P}}_n^0$	1 W
B	50 MHz	$P_{\mathrm{n}}^{\max}$	1.5 W
$P_m^{\max}$	1 W	σ	-30 dB
H	100 m	π	2.5
R	100 m	τ	5×10^{-2}
θ	1000		

2) Performance metrics of the experiment. To compare the advantages of our scheme, three performance metrics are employed:

- *The average utility*: The average utility includes the average secrecy rate and average overlapping area of UAVs.
- *Convergence of Algorithms*: The number of iterations when the iterative algorithm reaches convergence.
- *Trajectory, velocity and transmission power of the UAVs*: The influence of the UAVs' dynamically adjusting trajectory, velocity, and transmission power on system performance.

3) Compared baselines. Inspired by [32], [39], the proposed joint optimization (JO) scheme is compared with three baselines as follows:

- *Selected Closest UGV (SCU)*: To improve the transmission rate of offloading data, the UAVs offload their tasks to the nearest UGV. The trajectories and transmission power of UAVs and transmission power of AN are optimized.
- *Fixed Trajectory (FT)*: Each UAV flies from a given origin to the end according to the initial circular trajectory $\mathbf{q}_m^0 = [x_m + r \cos \theta_i, y_m + r \sin \theta_i]^\top, i = 1, ..., I$, where

---
[1] http://kolntrace.project.citi-lab.fr/

$\theta_i \triangleq 2\pi \frac{i-1}{I-1}, \forall i$. The UAVs' transmission power, AN transmission power, and UGV selection are optimized.

- *Fixed Transmission Power of UAVs (FTPU)*: The UAVs' transmission power are fixed at 0.8 W, and UAVs' trajectories, AN transmission power, and selection of UGVs are optimized.

The above baselines can be implemented by adjusting Algorithms 1 and Algorithms 2.

B. Convergence and Performance Evaluation

Fig. 4 shows the convergence of the proposed JO scheme and the three baselines at $T = 50$ s, $\mathcal{M} = 2$ and, $\mathcal{K} = 3$. As depicted in Fig. 4, the average utility of all schemes first shows an upward trend and then converges to a constant within a few iterations as the number of iterations increases. Furthermore, it is evident that the average utility of our JO scheme consistently outperforms the baseline scheme significantly. In detail, the proposed scheme achieves approximately 22.1%, 6.2%, and 30.4% performance gains over the SCU scheme, FTPU scheme, and FT scheme, respectively.

In Fig. 5, we focus on the average utility versus flight duration T when $\mathcal{M} = 2$ and the $\mathcal{K} = 3$. The FT scheme maintains a constant average utility, while the JO, SCU, and FTPU schemes show significant performance improvements as the flight duration T increases. The reason behind this trend is that with longer T, the UAVs have more time to approach the selected UGV and fly away from the Eves in the JO, SCU, and FTPU schemes. This allows them to achieve better transmission rates by establishing stronger channel links. Among the schemes, the JO scheme achieves the highest average utility. This is because it can dynamically adjust the UAVs' trajectories and transmission power, and select the UGV with the best channel links. More precisely, to get a better LoS link, the UAVs increase (decrease) the transmission power when it flies closer to (farther away from) the selected UGV. The FTPU scheme lacks the ability to dynamically adjust the UAVs' transmission power, which can impact the achievable transmission rate of the UGV. As for the FT scheme, its fixed UAV trajectories make the flight duration have no influence on its average utility.

In Fig. 6, we measure the average utility of the aforementioned four schemes versus different AN transmission power of the UGVs when $\mathcal{M} = 2$, $T = 50$s and $\mathcal{K} = 3$. As presented by Fig. 6, the performance of all schemes initially increases and then stabilizes as AN transmission power increases. This behavior can be attributed to the quality of the wiretap channel, which rapidly deteriorates as the AN transmission power is small. As the AN transmission power increases, the eavesdropper's rate approaches zero when the AN transmission power is sufficiently large. Additionally, it is noteworthy that the JO scheme consistently outperforms the other three baseline schemes, which proves the benefits of the joint optimization of UAVs' trajectory and transmission power, AN transmission power, and UGVs selection. Furthermore, Fig. 6 demonstrates that the FT scheme performs the worst among all the schemes. This indicates that leveraging UAVs' mobility to dynamically adjust their trajectories for optimizing

LoS links is more effective. Compared to SCU, FTPU, and FT schemes, the proposed JO scheme improves the average utility by approximately 21.4%, 6.2%, and 30.7%, respectively.

Fig. 7 quantifies the convergence of the JO scheme versus T with $\mathcal{M} = 2$ and $\mathcal{K} = 3$. As shown in Fig. 7, the JO scheme quickly converges within six iterations with different flight duration. Moreover, it can be observed that the average utility increases as flight duration T increases. The is because longer flight durations provide UAVs with more time and freedom to adjust their flight velocities and trajectories. By flying closer to the selected UGV and farther away from the eavesdroppers, the UAVs can establish and maintain high-quality channel links for a greater number of time slots. Therefore, the system performance improves with larger values of T. In addition, the average utility at duration $T = 75$ s is similar to that $T = 100$ s. The reason is that when T is sufficiently large, the UAVs' trajectories only require minor adjustments. This indicates that the proposed JO scheme can flexibly adjust the UAVs' trajectories, velocity, and transmission power to achieve optimal performance, as discussed in the following simulations.

In Fig.8, the optimized trajectories of the UAVs for the JO scheme are shown for different flight durations T. The UGVs' trajectories are denoted by q_N, the initial trajectories of the UAVs are marked by $\circ$, and the estimated locations of the Eves are marked by $\star$. As T increases, the UAV_1 initially follows the selected UGV as closely as possible to reduce the distance of the main channel. Then, it flies away from the Eve_1 to increase the distance of the wiretap channel. Finally, it flies to end point while bypassing Eve_1. On the other hand, the UAV_2 initially flies away from Eve_2 to increase the distance of the wiretap channel. Then, it follows the selected UGV as long as possible to reduce the distance of the main channel. Finally, it reaches to end point while bypassing the Eve_3. These optimized trajectories indicate that the UAVs can adjust their paths to improve the quality of the channel links. By flying closer to the selected UGVs and farther away from the eavesdroppers, the UAVs can achieve highly secure communication and better monitoring performance. Furthermore, Fig. 8 also demonstrates that as the flight duration T increases, the UAVs can flexibly adjust their trajectories to fly closer to the selected UGVs and further away from the Eves simultaneously. This is evident from the higher density of sampled points around each selected UGV in the trajectories, indicating that the UAVs spend more time in close proximity to the UGVs. Such observations further validate the critical role of optimizing the UAVs' trajectories in achieving highly secure communication and better monitoring performance.

Fig. 9 illustrates the velocity of UAV_1 for different flight durations T versus time slots I. When the flight duration is relatively short, such as $T = 50$s, the UAV flies with its maximum velocity $V_{\max}$ for most of the time slots to ensure it reaches the destination on time. As the flight duration increases, such as in the case of $T = 75$s, the UAVs have more flexibility in trajectory optimization, including adjusting their velocity. It can be observed that the UAVs fly at a lower velocity and wander around the selected UGV when
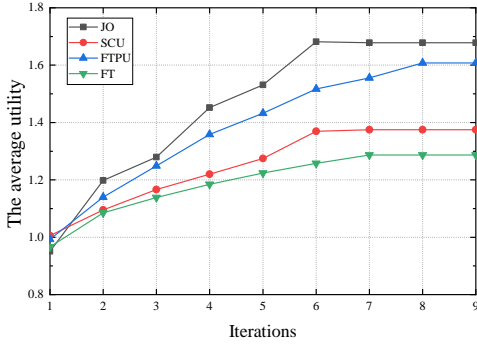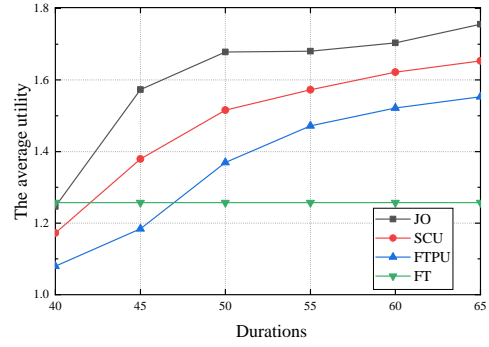
Fig. 4.   The average utility versus number of iterations

Fig. 5.   The average utility versus the flight duration of the UAVs T
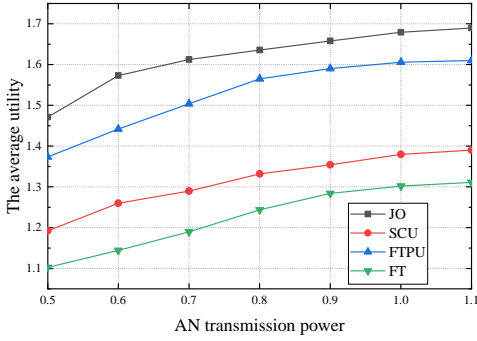

Fig. 6.   The average utility versus AN transmission power
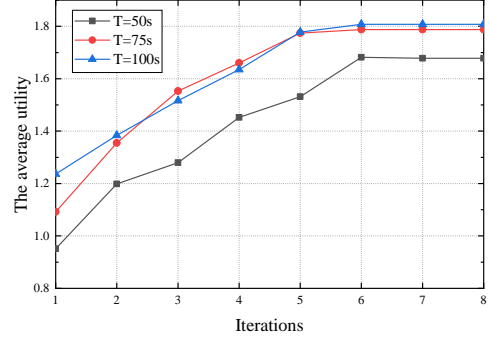

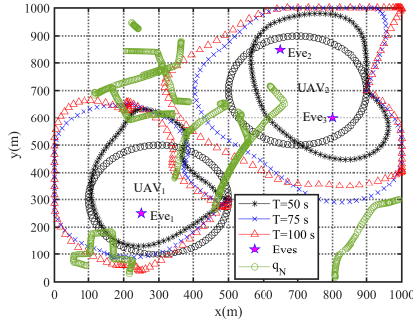Fig. 7.   The average utility versus the number of iterations.

Fig. 8.   The optimized trajectories of UAVs for different durations T.
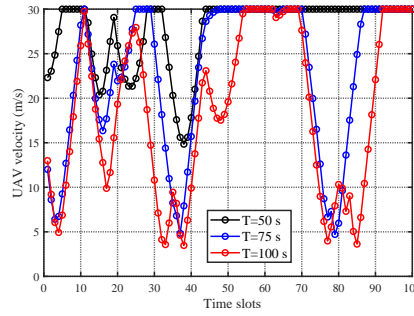

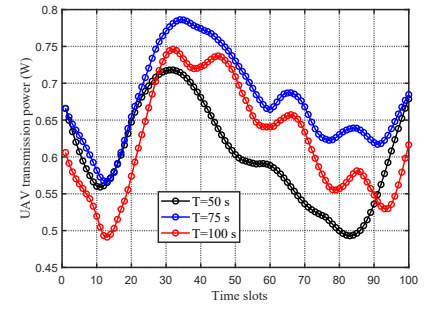Fig. 9.   Velocity of UAV$_1$ for different durations T versus time slots.

Fig. 10.   Transmission power of UAV$_1$ for different durations T versus time slots.

approaching it. This behavior allows them to spend more time in close proximity to the UGV, ensuring high-quality channel links for safe and secure information transmission. According to Fig. 9, for the case of $T = 100$s, the UAV has sufficient time to return to the destination. When the UAV flies close to the selected UGV, it reduces its velocity to 5 m/s to stay close to the UGV as long as possible. Meanwhile, the UAV flies at its maximum velocity when moving away from the Eves. This behavior is aimed at maximizing the duration of secure communication by establishing and maintaining high-quality channel links.

Fig. 10 exhibits the transmission power of the UAV$_1$ for different flight duration T versus the time slots. It is worth noting that the variation trend of the UAV transmission power is similar across different duration T. As can be seen from time slots 10 to 20 and 80 to 90, the UAV flies close to the

Eve$_1$, which poses a high potential for confidential information leakage. To mitigate this risk, the UAV decreases its transmission power to reduce the instantaneous eavesdropper rate, as defined in Eq.(5). From Fig. 8∼10, we can observe that when the UAV flies close to the selected UGV and away from the Eve$_1$ during time slots 30 to 40, the optimal channel quality is created through a combination of reducing the UAVs' velocity and increasing its transmission power. In addition, when the UAV is located between two UGVs during time slots 50 to 70, it flies at its maximum velocity to get close to the selected UGV and ensure wireless communication security. However, since the UAV is close to Eve$_1$ at the same time, it offloads tasks by using optimal transmission power. Thus, we can induce that our proposed scheme improves system performance effectively.

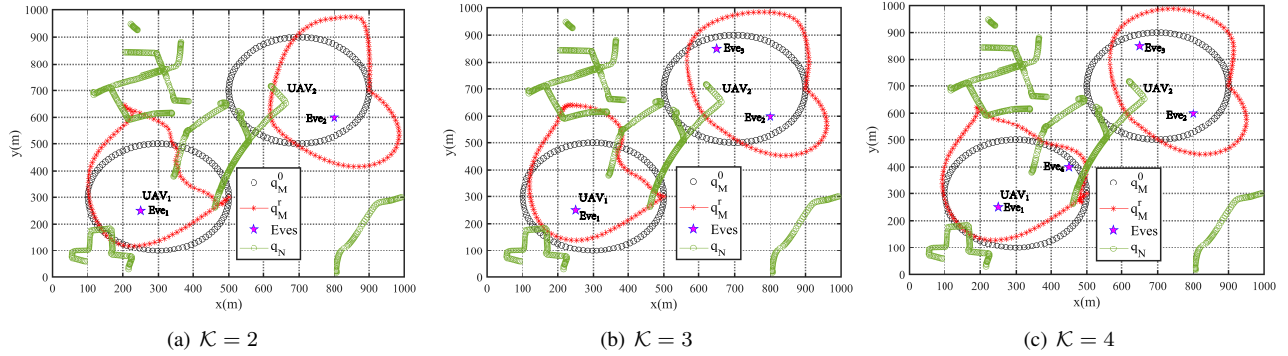From Figs. 8, 9, and 10, the observations indicate our

Fig. 11. The optimized trajectories of two UAVs for different numbers of Eves.
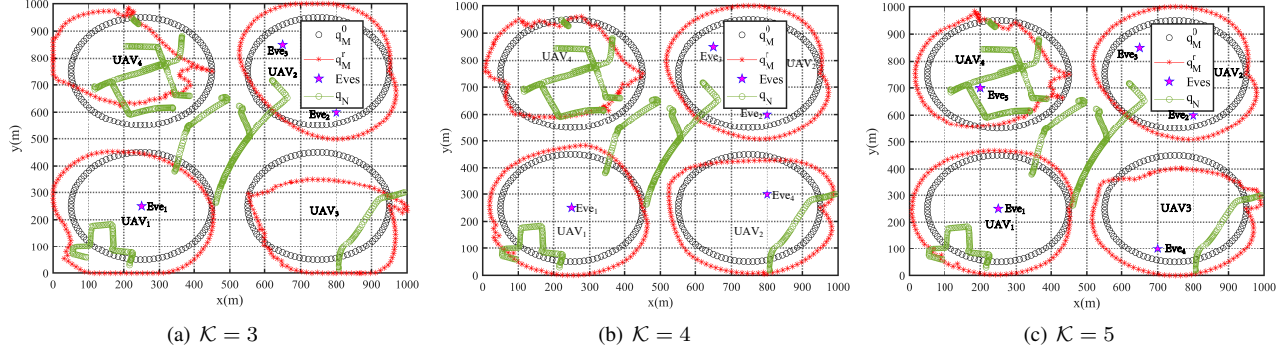

Fig. 12. The optimized trajectories of four UAVs for different numbers of Eves.

proposed scheme allows the UAV to adapt its transmission power according to the specific scenario and optimize the overall system performance by ensuring secure communication and simultaneously mitigating the risk of eavesdropping.

C. The UAVs Trajectories

In Fig. 11, we vary the number of Eves $\mathcal{K}$ from 2 to 4 to quantify its impact on the performance of the systems explicitly with $\mathcal{M} = 2$ and $T = 50$s. The q_M^0 is the initial trajectories of the UAV, the q_M^r represents the optimized trajectories of the UAV, while the q_N denotes the trajectories of the UGV. As the number of Eves increases, we can see from the trajectories that the UAVs modify their paths to fly as close to the selected UGV as possible while avoiding the Eves. This behavior aims to maximize the security of the communication links between the UAV and UGV. When $\mathcal{K}$ is set to 2, 3, and 4, the average utility ϑ is 1.70, 1.67, and 1.65, respectively. It is evident that the average utility decreases as the number of Eves increases. This decrease can be attributed to the fact that more eavesdroppers result in a larger amount of stolen information, as indicated by Eq. (18). Although the average utility experiences a slight decline as the number of eavesdroppers increases, the proposed secure offloading scheme still achieves better performance in the presence of multiple Eves.

Fig. 12 depicts the optimized trajectories of four UAVs with $\mathcal{K}$ growing from 3 to 5 and $T = 50$s. These figures demonstrate that the proposed secure offloading scheme effectively avoids potential collisions among UAVs. Meanwhile, the UAVs try to fly away from each other to reduce channel interference based on Eq.(4). Additionally, similarly

to Fig. 11, the UAVs also fly away from Eves and close to the selected UGV to increase the average utility of the system by improving the quality of channel links. These results highlight the effectiveness of the proposed joint optimization scheme in managing multiple UAV systems. The scheme successfully minimizes collisions, reduces interference, and ensures the security of communication links by avoiding Eves and optimizing channel quality.

Overall, the proposed JO scheme proves to be highly effective, offering superior performance compared to other benchmarks, even in complex scenarios involving multiple Eves and multiple UAVs.

VI. CONCLUSIONS

In this paper, the secure computation tasks offloading and monitoring scheme for the MEC-based UAV-UGV collaborate framework with multiple UAVs, UGVs, and Eves has been investigated. The objective is to maximize the minimum average utility of systems by jointly optimizing various parameters such as UAVs' trajectories and transmission power, AN transmission power, CPU frequency of UAVs and UGVs, and selection of UGVs while considering constraints on latency, power, velocity, anti-collision, and distance. To deal with the complexity of the problem, the original optimization problem is first divided into six sub-problems. Afterward, we proposed an efficient BCD-based iterative algorithm for solving the optimization problem. Moreover, the convergence and complexity of algorithm 2 have been analyzed. Extensive simulation with large-scale scenarios demonstrates that the JO scheme can improve the average utility by up to 30.4%, compared to three benchmarks. There are several watchable directions in

further work, including optimizing the UGVs' trajectories, extending the current work into scenarios with cooperation surveillance between UGVs and UAVs, and studying workload and collaboration balancing among the entities.

APPENDIX A

In this section, the SCA technique [36] is used to derive the convex approximation problem (21). Recall that any convex function is globally low-bounded by its first-order Taylor expansion at any point [40]. Given the local point $\{\mathbf{q}_m^r(i)\}$ over the rth iteration, we have the following lower bound of $R_{mn}(i)$ as follow [36]:

$$
\begin{aligned}
R_{mn}(i) &= \log_2\left(1 + \frac{p_m(i)h_{mn}(i)}{\sum\limits_{j\in\mathcal{M},j\neq m} p_j(i)h_{jn}(i)+\sigma^2}\right) \\
&\geqslant \log_2\left(1 + \frac{\frac{p_m(i)\eta_0}{H^2+\|\mathbf{q}_m^r(i)-\bar{\mathbf{q}}_n(i)\|^2}}{\sum\limits_{j\in\mathcal{M},j\neq m} \frac{p_j(i)\eta_0}{\|\mathbf{q}_j^r(i)-\bar{\mathbf{q}}_n(i)\|^2}+\sigma^2}\right) \\
&\quad + (\mathbf{q}_m(i)-\mathbf{q}_m^r(i))^\top\left(\frac{\delta R_{mn}(i)}{\delta h_{mn}(i)}\frac{\delta h_{mn}(i)}{\delta\mathbf{q}_m(i)}\bigg|_{\mathbf{q}_m=\mathbf{q}_m^r}\right) \\
&\quad + \sum_{j\in\mathcal{M},j\neq m}(\mathbf{q}_j(i)-\mathbf{q}_j^r(i))^\top\left(\frac{\delta R_{mn}(i)}{\delta h_{jn}(i)}\frac{\delta h_{jn}(i)}{\delta\mathbf{q}_j(i)}\bigg|_{\mathbf{q}_j=\mathbf{q}_j^r}\right) \\
&\triangleq \bar{R}_{mn}(i),
\end{aligned}
\tag{32}
$$

where $\frac{\delta R_{mn}(i)}{\delta h_{jn}(i)} = \frac{1}{2^{R_{mn}(\mathbf{Q})}\ln 2}\frac{-\sum\limits_{j\in\mathcal{M},j\neq m}p_j(i)p_m(i)h_{mn}(i)}{(p_j(i)h_{jn}(i)+\sigma^2)^2}$, $\frac{\delta R_{mn}(i)}{\delta h_{mn}(i)} = \frac{1}{2^{R_{mn}(\mathbf{Q})}\ln 2}\frac{p_m(i)}{\sum\limits_{j\in\mathcal{M},j\neq m}p_j(i)h_{jn}(i)+\sigma^2}$, $\frac{\delta h_{mn}(i)}{\delta\mathbf{q}_m(i)} = \frac{-2\eta_0(\mathbf{q}_m(i)-\bar{\mathbf{q}}_n(i))}{(H^2+\|\mathbf{q}_m(i)-\bar{\mathbf{q}}_n(i)\|^2)^2}$, $\frac{\delta h_{jn}(i)}{\delta\mathbf{q}_j(i)} = \frac{-2\eta_0(\mathbf{q}_j(i)-\bar{\mathbf{q}}_n(i))}{(H^2+\|\mathbf{q}_j(i)-\bar{\mathbf{q}}_n(i)\|^2)^2}$.

To compute the convex relaxation of $\bar{R}_{mk}^{up}(i)$ by the SCA technique, we define an auxiliary variable $S_{mk}(i) \leq (\|\mathbf{q}_m(i)-\widetilde{\mathbf{q}}_k(i)\|-\Delta Q)^2$ and apply a Taylor expansion at $\{\mathbf{q}_m^r(i)\}$. $\bar{R}_{mk}^{up}(i)$ can be rewritten as:

$$
\bar{R}_{mk}^{up}(i) = \log_2\left(1 + \frac{\varepsilon_{mk}(i)p_m(i)\eta_0}{S_{mk}(i)}\right) \triangleq \bar{R}_{mk}^{up}(i), \tag{33}
$$

where $\varepsilon_{mk}(i) = \frac{1}{\sum\limits_{j\in\mathcal{M},j\neq m}p_j(i)h_{jk}^*(i)+\sum\limits_{n\in\mathcal{N}}\widetilde{h}_{nk}^*(i)p_n^{an}(i)+\sigma^2}$ and $S_{mk}(i) \leq (\|\mathbf{q}_m^r(i)-\widetilde{\mathbf{q}}_k(i)\|-\Delta Q)^2 + 2(\|\mathbf{q}_m(i)-\widetilde{\mathbf{q}}_k(i)\|-\Delta Q)\frac{(\mathbf{q}_m^r(i)-\widetilde{\mathbf{q}}_k(i))^\top}{\|\mathbf{q}_m^r(i)-\widetilde{\mathbf{q}}_k(i)\|}(\mathbf{q}_m(i)-\mathbf{q}_m^r(i))$.

In the constraint (21h), by using the first-order Taylor expansion at the given point $\mathbf{q}_m^r(i)$ and $\mathbf{q}_j^r(i)$ to $\|\mathbf{q}_m^r(i)-\mathbf{q}_j^r(i)\|^2$, we have:

$$
\begin{aligned}
\|\mathbf{q}_m^r(i)-\mathbf{q}_j^r(i)\|^2 &\geqslant -\|\mathbf{q}_m^r(i)-\mathbf{q}_j^r(i)\|^2 + 2(\mathbf{q}_m^r(i) \\
&\quad - \mathbf{q}_j^r(i)(\mathbf{q}_m(i)-\mathbf{q}_j(i)),
\end{aligned}
\tag{34}
$$

Similarly, since $\|\mathbf{q}_m(i+1)-\mathbf{q}_m(i)\|^2$ is a convex in terms to $\mathbf{q}_m(i)$. By employing the first-order Taylor expansion at the given point $\mathbf{q}_m^r(i)$, we have:

$$
\begin{aligned}
\|\mathbf{q}_m^r(i+1)-\mathbf{q}_m^r(i)\|^2 &\geqslant -\|\mathbf{q}_m^r(i+1)-\mathbf{q}_m^r(i)\|^2 \\
&\quad + 2(\mathbf{q}_m^r(i+1)-\mathbf{q}_m^r(i))(\mathbf{q}_m(i+1)-\mathbf{q}_m(i)).
\end{aligned}
\tag{35}
$$

APPENDIX B

Eq. (23) shows a non-convex optimization problem. Next, the SCA technique is resort to get efficient approximation solution. Firstly, we rewrite $R_{mn}(i)$ as follows:

$$
R_{mn}(i) = \underbrace{\log_2\left(\sum_{m\in\mathcal{M}}p_m(i)h_{mn}(i)+\sigma^2\right)}_{I_1(i)} - \underbrace{\log_2\left(\sum_{l\in\mathcal{M},j\neq m}p_j(i)h_{jn}(i)+\sigma^2\right)}_{I_2(i)}. \tag{36}
$$

After that, we solve this subproblem by exploiting a similar approach mentioned in the previous section. In detail, we successively transform $I_2(i)$ into convex terms by applying the first-order Taylor expansions. The $\mathbf{P}_m^r = \{p_m^r(i)\}$ denotes the transmit power of UAV m in the rth iteration. $I_2(i)$ is given by:

$$
\begin{aligned}
I_2(i) &= \log_2\left(\sum_{j\in\mathcal{M},j\neq m}p_j^r(i)h_{jn}(i)+\sigma^2\right) \\
&\quad + \frac{\sum\limits_{j\in\mathcal{M},j\neq m}h_{jn}(i)(p_j(i)-p_j^r(i))}{\left(\sum\limits_{j\in\mathcal{M},j\neq m}p_j^r(i)h_{jn}(i)+\sigma^2\right)\ln 2},
\end{aligned}
\tag{37}
$$

To compute the convex relaxation of $\bar{R}_{mk}^{ub}(i)$, we use the similar steps above and rewrite it as:

$$
\begin{aligned}
\bar{R}_{mk}^{ub}(i) =& \underbrace{\log_2\left(p_m(i)\bar{h}_{mk}^{\max}(i)+\sum_{j\in\mathcal{M},j\neq m}p_j(i)\bar{h}_{jk}^{\min}(i)+\omega_{mk}\right)}_{I_3(i)} \\
&- \underbrace{\log_2\left(\sum_{j\in\mathcal{M},j\neq m}p_j(i)\bar{h}_{jk}^{\min}(i)+\omega_{mk}\right)}_{I_4(i)},
\end{aligned}
\tag{38}
$$

where $\omega_{mk} = \sum\limits_{n\in\mathcal{N}}p_n^{an}\widetilde{h}_{nk}^{\min}(i)+\sigma^2$. $I_3(i)$ is a convex upper bound expression based on the first-order Taylor expansion in terms of the transmission power of the UAV m in the rth iteration, which can be expressed as:

$$
\begin{aligned}
I_3(i) =& \log_2\left(p_m^r(i)\bar{h}_{mk}^{\max}(i)+\sum_{j\in\mathcal{M},j\neq m}p_j^r(i)\bar{h}_{jk}^{\min}(i)+\omega_{mk}\right) \\
&+ \frac{\bar{h}_{mk}^{\max}(i)(p_m(i)-p_m^r(i))+\sum\limits_{j\in\mathcal{M},j\neq m}\bar{h}_{jk}^{\min}(i)(p_j(i)-p_j^r(i))}{\left(p_m^r(i)\bar{h}_{mk}^{\max}(i)+\sum\limits_{j\in\mathcal{M},j\neq m}p_j^r(i)\bar{h}_{jk}^{\min}(i)+\omega_{mk}\right)\ln 2},
\end{aligned}
\tag{39}
$$

C ACKNOWLEDGEMENT

REFERENCES

[1] L. Gupta, R. Jain, and G. Vaszkun, "Survey of important issues in UAV communication networks," *IEEE Commun. Surv. Tutorials*, vol. 18, no. 2, pp. 1123–1152, 2016.

[2] T. Zhang, Y. Xu, J. Loo, D. Yang, and L. Xiao, "Joint computation and communication design for uav-assisted mobile edge computing in iot," *IEEE Trans. Ind. Informatics*, vol. 16, no. 8, pp. 5505–5516, 2020.

[3] N. H. Motlagh, M. Bagaa, and T. Taleb, "Uav-based iot platform: A crowd surveillance use case," *IEEE Commun. Mag.*, vol. 55, no. 2, pp. 128–134, 2017.

[4] A. Trotta, F. D'Andreagiovanni, M. D. Felice, E. Natalizio, and K. R. Chowdhury, "When uavs ride A bus: Towards energy-efficient city-scale video surveillance," in *2018 IEEE Conference on Computer Communications, INFOCOM 2018, Honolulu, HI, USA, April 16-19, 2018.* IEEE, 2018, pp. 1043–1051.

[5] J. Zhang, Z. Li, W. Xu, J. Peng, W. Liang, Z. Xu, X. Ren, and X. Jia, "Minimizing the number of deployed uavs for delay-bounded data collection of iot devices," in *40th IEEE Conference on Computer Communications, INFOCOM 2021, Vancouver, BC, Canada, May 10-13, 2021.* IEEE, 2021, pp. 1–10.

[6] S. Hu, W. Ni, X. Wang, A. Jamalipour, and D. Ta, "Joint optimization of trajectory, propulsion, and thrust powers for covert uav-on-uav video tracking and surveillance," *IEEE Trans. Inf. Forensics Secur.*, vol. 16, pp. 1959–1972, 2021.

[7] W. Chen, Z. Su, Q. Xu, T. H. Luan, and R. Li, "Vfc-based cooperative UAV computation task offloading for post-disaster rescue," in *39th IEEE Conference on Computer Communications, INFOCOM 2020, Toronto, ON, Canada, July 6-9, 2020.* IEEE, 2020, pp. 228–236.

[8] T. Bai, J. Wang, Y. Ren, and L. Hanzo, "Energy-efficient computation offloading for secure uav-edge-computing systems," *IEEE Trans. Veh. Technol.*, vol. 68, no. 6, pp. 6074–6087, 2019.

[9] P. A. Apostolopoulos, E. Tsiropoulou, and S. Papavassiliou, "Risk-aware data offloading in multi-server multi-access edge computing environment," *IEEE/ACM Trans. Netw.*, vol. 28, no. 3, pp. 1405–1418, 2020.

[10] M. Chen, A. Liu, W. Liu, K. Ota, M. Dong, and N. Xiong, "Rdrl a recurrent deep reinforcement learning scheme for dynamic spectrum access in reconfigurable wireless networks," *IEEE Transactions on Network Science and Engineering*, 2021.

[11] M. Chen, W. Liu, T. Wang, S. Zhang, and A. Liu, "A game-based deep reinforcement learning approach for energy-efficient computation in mec systems," *Knowledge-Based Systems*, vol. 235, p. 107660, 2022.

[12] Q. Yuan, H. Zhou, J. Li, Z. Liu, F. Yang, and X. S. Shen, "Toward efficient content delivery for automated driving services: An edge computing solution," *IEEE Netw.*, vol. 32, no. 1, pp. 80–86, 2018.

[13] Y. Zhou, C. Pan, P. L. Yeoh, K. Wang, M. Elkashlan, B. Vucetic, and Y. Li, "Secure communications for uav-enabled mobile edge computing systems," *IEEE Trans. Commun.*, vol. 68, no. 1, pp. 376–388, 2020.

[14] C. J. Li and H. Ling, "Synthetic aperture radar imaging using a small consumer drone," in *2015 IEEE international symposium on antennas and propagation USNC/URSI national radio science meeting*, 2015, pp. 685–686.

[15] X. Sun, D. W. K. Ng, Z. Ding, Y. Xu, and Z. Zhong, "Physical layer security in UAV systems: Challenges and opportunities," *IEEE Wirel. Commun.*, vol. 26, no. 5, pp. 40–47, 2019.

[16] J. Tang, G. Chen, and J. P. Coon, "Secrecy performance analysis of wireless communications in the presence of UAV jammer and randomly located UAV eavesdroppers," *IEEE Trans. Inf. Forensics Secur.*, vol. 14, no. 11, pp. 3026–3041, 2019.

[17] N. Wang, P. Wang, A. Alipour-Fanid, L. Jiao, and K. Zeng, "Physical-layer security of 5g wireless networks for iot: Challenges and opportunities," *IEEE Internet Things J.*, vol. 6, no. 5, pp. 8169–8181, 2019.

[18] X. He, R. Jin, and H. Dai, "Physical-layer assisted secure offloading in mobile-edge computing," *IEEE Trans. Wirel. Commun.*, vol. 19, no. 6, pp. 4054–4066, 2020.

[19] N. Zhao, X. Pang, Z. Li, Y. Chen, F. Li, Z. Ding, and M. Alouini, "Joint trajectory and precoding optimization for uav-assisted NOMA networks," *IEEE Trans. Commun.*, vol. 67, no. 5, pp. 3723–3735, 2019.

[20] X. Sun, D. W. K. Ng, Z. Ding, Y. Xu, and Z. Zhong, "Physical layer security in UAV systems: Challenges and opportunities," *IEEE Wirel. Commun.*, vol. 26, no. 5, pp. 40–47, 2019.

[21] Y. Zhou, F. Zhou, H. Zhou, D. W. K. Ng, and R. Q. Hu, "Robust trajectory and transmit power optimization for secure uav-enabled cognitive radio networks," *IEEE Trans. Commun.*, vol. 68, no. 7, pp. 4022–4034, 2020.

[22] N. Nguyen, H. Q. Ngo, T. Q. Duong, H. D. Tuan, and K. Tourki, "Secure massive MIMO with the artificial noise-aided downlink training," *IEEE J. Sel. Areas Commun.*, vol. 36, no. 4, pp. 802–816, 2018.

[23] W. Wang, X. Li, R. Wang, K. Cumanan, W. Feng, Z. Ding, and O. A. Dobre, "Robust 3d-trajectory and time switching optimization for dual-uav-enabled secure communications," *IEEE Journal on Selected Areas in Communications*, pp. 1–1, 2021.

[24] Y. Mao, J. Zhang, and K. B. Letaief, "Joint task offloading scheduling and transmit power allocation for mobile-edge computing systems," in *2017 IEEE Wireless Communications and Networking Conference, WCNC 2017, San Francisco, CA, USA, March 19-22, 2017.* IEEE, 2017, pp. 1–6.

[25] T. Bai, C. Pan, Y. Deng, M. Elkashlan, A. Nallanathan, and L. Hanzo, "Latency minimization for intelligent reflecting surface aided mobile edge computing," *IEEE J. Sel. Areas Commun.*, vol. 38, no. 11, pp. 2666–2682, 2020.

[26] C. Zhan and Y. Zeng, "Energy-efficient data uploading for cellular-connected UAV systems," *IEEE Trans. Wirel. Commun.*, vol. 19, no. 11, pp. 7279–7292, 2020.

[27] Z. Ning, P. Dong, M. Wen, X. Wang, L. Guo, R. Y. Kwok, and H. V. Poor, "5g-enabled uav-to-community offloading: Joint trajectory design and task scheduling," *IEEE J. Sel. Areas Commun.*, vol. 39, no. 11, pp. 3306–3320, 2021.

[28] M. Li, N. Cheng, J. Gao, Y. Wang, L. Zhao, and X. Shen, "Energy-efficient uav-assisted mobile edge computing: Resource allocation and trajectory optimization," *IEEE Trans. Veh. Technol.*, vol. 69, no. 3, pp. 3424–3438, 2020.

[29] J. Zhang, L. Zhou, Q. Tang, E. C. H. Ngai, X. Hu, H. Zhao, and J. Wei, "Stochastic computation offloading and trajectory scheduling for uav-assisted mobile edge computing," *IEEE Internet Things J.*, vol. 6, no. 2, pp. 3688–3699, 2019.

[30] Y. Cai, F. Cui, Q. Shi, M. Zhao, and G. Y. Li, "Dual-uav-enabled secure communications: Joint trajectory design and user scheduling," *IEEE J. Sel. Areas Commun.*, vol. 36, no. 9, pp. 1972–1985, 2018.

[31] J. Li, H. Kang, G. Sun, S. Liang, Y. Liu, and Y. Zhang, "Physical layer secure communications based on collaborative beamforming for UAV networks: A multi-objective optimization approach," in *40th IEEE Conference on Computer Communications, INFOCOM 2021, Vancouver, BC, Canada, May 10-13, 2021.* IEEE, 2021, pp. 1–10.

[32] Y. Cai, Z. Wei, R. Li, D. W. K. Ng, and J. Yuan, "Joint trajectory and resource allocation design for energy-efficient secure UAV communication systems," *IEEE Trans. Commun.*, vol. 68, no. 7, pp. 4536–4553, 2020.

[33] X. Gu, G. Zhang, M. Wang, W. Duan, M. Wen, and P. Ho, "Uav-aided energy-efficient edge computing networks: Security offloading optimization," *IEEE Internet Things J.*, vol. 9, no. 6, pp. 4245–4258, 2022.

[34] Z. Lin, M. Lin, B. Champagne, W. Zhu, and N. Al-Dhahir, "Secure beamforming for cognitive satellite terrestrial networks with unknown eavesdroppers," *IEEE Syst. J.*, vol. 15, no. 2, pp. 2186–2189, 2021.

[35] M. Cui, G. Zhang, Q. Wu, and D. W. K. Ng, "Robust trajectory and transmit power design for secure UAV communications," *IEEE Trans. Veh. Technol.*, vol. 67, no. 9, pp. 9042–9046, 2018.

[36] Q. Wu, Y. Zeng, and R. Zhang, "Joint trajectory and communication design for multi-uav enabled wireless networks," *IEEE Trans. Wirel. Commun.*, vol. 17, no. 3, pp. 2109–2121, 2018.

[37] J. Qiao, H. Zhang, F. Zhao, and D. Yuan, "Secure transmission and self-energy recycling with partial eavesdropper CSI," *IEEE J. Sel. Areas Commun.*, vol. 36, no. 7, pp. 1531–1543, 2018.

[38] C. Zhong, J. Yao, and J. Xu, "Secure UAV communication with cooperative jamming and trajectory control," *IEEE Commun. Lett.*, vol. 23, no. 2, pp. 286–289, 2019.

[39] H. Lee, S. Eom, J. Park, and I. Lee, "Uav-aided secure communications with cooperative jamming," *IEEE Trans. Veh. Technol.*, vol. 67, no. 10, pp. 9385–9392, 2018.

[40] C. Lemaréchal, "S. boyd, l. vandenberghe, convex optimization, cambridge university press, 2004 hardback, ISBN 0 521 83378 7," *Eur. J. Oper. Res.*, vol. 170, no. 1, pp. 326–327, 2006.
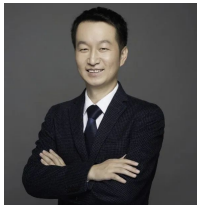
PeiPei Chen received the M.E. degree in computer science and technology from Guangxi University, Nanning, China, in 2020. She is currently pursuing the Ph.D. degree with the control science and engineering, National University of Defense Technology, Changsha, China. Her research interests include convex and nonconvex optimization, physical layer security, and unmanned aerial vehicle (UAV) communications.

Yuchen Sun received the B.S. degree in Telecommunication Engineering from the Huazhong University of Science and Technology, Wuhan, China, in 2018. He has been with the School of System Engineering, National University of Defense Technology, Changsha, since 2018, where he is currently pursuing the Ph.D degree. His research interests include Mobile Edge Computing, Dynamic Neural Networks and Wireless Indoor Localization.

Lailong Luo received his B.S., M.S. and Ph.D degree at the College of Systems Engineering from National University of Defence Technology, Changsha, China, in 2013, 2015, and 2019 respectively. He is currently an associate professor in the School of Systems, National University of Defense Technology, Changsha, China. His research interests include data structure and distributed networking systems.

Deke Guo received the B.S. degree in industry engineering from the Beijing University of Aeronautics and Astronautics, Beijing, China, in 2001, and the Ph.D. degree in management science and engineering from the National University of Defense Technology, Changsha, China, in 2008. He is currently a Professor with the College of System Engineering, National University of Defense Technology, and is also with the College of Intelligence and Computing, Tianjin University. His research interests include distributed systems, data centre networking, wireless and mobile systems, and interconnection networks. He is a senior member of the IEEE and a member of the ACM.

Xinyi Li is a lecturer at National Unversity of Defense Technology. He obtained his Ph.D at University of Amsterdam and his master's and bachelor's degree at National Unversity of Defense Technology. His research interests include natural language processing and information retrieval.

Xueshan Luo received his B.E. degree in Information Engineering from Huazhong Institute of Technology, Wuhan, China, in 1985, and his M.S. and Ph.D degrees in System Engineering from the National University of Defense Technology, Changsha, China, in 1988 and 1992, respectively. Currently, he is a professor of College of Systems Engineering, National University of Defense Technology. His research interests are in the general areas of information systems and operation research.